A Coupled Thermal-Displacement Simulation Model for Friction Stir Welding of Thin Aluminium Sheets

M. Tawadros[1] M. Harraz[2]
[1,2] Faculty of Engineering and Materials Science
[1, 2] German University in Cairo, Egypt

Abstract— Friction stir welding is a novel innovative solid state welding process that is mainly used nowadays to join aluminium sheets. Due to the time and economic constraints, the verification of the experimental work using appropriate simulation models has become essential to reduce the hassle of the practical approaches. Many simulation models were designed to verify different process parameters but very little of the simulation approaches were conducted on the complete process. This present work focuses on a complete coupled thermal-displacement analysis model that is simulating the whole friction stir welding process from the "penetration" to the final "feed step". For the simulation process two models were designed using Abaqus-Explicit, the first simulating the "penetration" and "dwelling" processes only and the second simulating "feed steps" as well. The results of the simulation models are compared and calibrated with previous experimental work that is done on friction stir butt welded 1.5 mm aluminium sheets A6061-T6. The comparison of the experimental and simulation data has shown 95% matching of the results especially for the temperature distribution and shape of deformation obtained by the friction stir welding tool during the penetration process. The designed simulation model is therefore a proven consistent tool for simulating the unpredictable process parameters of the friction stir welding for a reliable optimization process.

Key words: Simulation, FSW, Aluminium

I. INTRODUCTION AND STATE OF THE ART

Friction Stir Welding (FSW) is a modern welding technique that is mainly used for joining heat sensitive metals such as aluminum alloys [1]. FSW as shown in Fig. 1 involves three main steps, the first is known as the penetration of the probe and partially the shoulder of the rotating tool into the plates or sheets to be joined together. The second step known as dwelling is the continuous rotation of the tool for some time just long enough to softens and plasticize the material. The final step is known as the feed step where the tool is moved transversely along the joining line between the two plates to be joined together [2]. During these three steps, there are many aspects related to the process that are not fully understood or predictable. The objective of the present work is therefore to build a complete fully coupled thermo-mechanical model for simulating the whole process of FSW from the penetration step till the final feed step, and secondly comparing the results obtained from the model with results obtained from experimental work under the same circumstances. In the way of reaching this objective a fully coupled three-dimensional solid mechanical model has been built using Abaqus-Explicit software with arbitrary Lagrange-Eulerian (ALE) mesh type that facilitates the simulation of severe deformation. Secondly an experimental work was done on a FSW machine using the same parameters from the simulation model and the heat distribution around the tool was recorded using a thermal camera for the calibration purposes. It is not claimed to be the overall thermo-mechanical state present during the real welding process, as modeling the whole processes in one model [3] cause severe deformation in the mesh after the dwelling step, which may not lead to a full deposition process of the material behind the tool [3].

Fig. 1: Layout of the main FSW steps

II. SIMULATION METHODOLOGY

In this paper, a fully coupled thermal-displacement simulation was used to analyze and solve both thermal and mechanical responses of FSW process. The FSW involves heating due to friction between the tool and the work-piece and inelastic deformation of the metal, in which properties of the metal are altered. Therefore, in the analysis, the thermal and mechanical solutions must be obtained at the same time. In fully coupled thermal-displacement formulation, the stress analysis depends on the temperature distribution and the temperature distribution depends on the stress solution, as each of them is related to the other and must be obtained simultaneous [4].

In Abaqus-Explicit the heat transfer equations are defined using the "explicit forward-difference time integration" rule [4].

$$T^{N}_{(i+1)} = T^{N}_{i} + \Delta t_{(i+1)} T'^{N}_{(i)} \qquad (2.1)$$

Where T^N the temperature at node N, t is the time and the subscript i refer to an increment number in an explicit dynamic step. The forward-difference integration is explicit in the sense that no equations need to be solved when a lumped capacitance matrix is used. The current temperatures are obtained using known values of $T'^{N}_{(i)}$ are computed at the beginning of the increment by

$$T'^{N}_{(i)} = (C^{NJ})^{-1}(P^{J}_{(i)} - F^{J}_{(i)}) \qquad (1.2)$$

Where C^{NJ} is the lumped capacitance matrix, P^J is the applied nodal force vector.

Also in Abaqus-Explicit dynamics analysis procedure is based upon the applying of an "explicit

integration" rule together with the use of "diagonal ("lumped") element mass" matrices. The equations of motion for the body are integrated using the "explicit central-difference integration" rule [5]

$$U'^{N}_{(i+\frac{1}{2})} = U'^{N}_{(i-\frac{1}{2})} + \frac{\Delta t_{(i+1)} + \Delta t_i}{2} U''^{N}_{(i)} \quad (2.3)$$

$$U^{N}_{(i+1)} = U^{N}_{(i)} + \Delta t_{(i+1)} U'^{N}_{(i+\frac{1}{2})} \quad (2.4)$$

Where U^N is the displacement, t is time and the subscript i refers to the increment number in an explicit dynamics step. The central-difference integration operator is explicit in the sense that the kinematic state is advanced using known values of $U''^{N}_{(i-\frac{1}{2})}$ and $U''^{N}_{(i)}$ from the previous increment.

The explicit integration rule by itself does not give the computational efficiency needed with the explicit dynamics procedure. The key to the computational efficiency of the explicit procedure is the use of diagonal element mass matrices because the accelerations at the beginning of the increment are computed by

$$U''^{N}_{(i)} = (M^{NJ})^{-1}(P^{J}_{(i)} - I^{J}_{(i)}) \quad (2.5)$$

Where M^{NJ} is the mass matrix, $P^{J}_{(i)}$ is the applied load vector, and $I^{J}_{(i)}$ is the internal force vector in this case it is the inertia. A lumped mass matrix is used because its inverse is simple to compute and because the vector multiplication of the mass inverse by the inertial force requires only *n* operations, where *n* is the number of degrees of freedom in the model. The explicit procedure requires no iterations and no tangent stiffness matrix. The internal force vector $I^{J}_{(i)}$ is assembled from contributions from each element such that a global stiffness matrix need not before. For the material model the Johnson-Cook plasticity model is a constitutive model that is mainly designed for computational aims for material subjected to large strain, high strain rates at elevated temperatures, which is relevant to be used in this work as in friction stir welding temperature increases along with high deformation. By this model the yield stress and the radius of the Von-Mises cylinder changes with the change of the strain rate and temperature. Material softening and strain hardening are considered to model the change in the response of the material. The main parameters that Johnson-Cook model consider are strain hardening, strain rate effects and softening of the material at higher temperatures, all these 3 effects are considered. In equation 2.6 the Johnson-Cook constitutive model [6]:

$$\sigma_y = \left[A + B\left(\varepsilon^{P}_{eff}\right)^{N}\right](1 + C ln\varepsilon')[1 - (T_H)^{M}] \quad (2.6)$$

σ_y is the material yield strength.

ε^{P}_{eff} is the effective plastic strain.

$\varepsilon' = \frac{\varepsilon'^{p}_{eff}}{\varepsilon'_o}$ where ε'_o is the strain rate used to determine A, B & N.

T_H is the homologous temperature = $\frac{T - T_R}{T_m - T_R}$

T_M is the melting temperatures assigned.

T_R is the reference temperature when determining A, B and N.

$\Delta T = \frac{1}{\rho C_p} \int \sigma d\varepsilon^{p}_{eff}$ Where ρ is mass density, T is the temperature and C_p is the metal specific heat.

A, B, N, C and M are material characteristics measured at temperature called "transition temperature" the above yield strength portion of the Johnson-Cook constitutive model has five parameters: A, B, N, C, and M, and three material characteristics: ρ, C_p and T_M in addition to elastic properties are required to input for analysis.

Johnson-Cook material properties used are shown in TABLE I, concerning other properties they were added as function of temperature as shown in the table [7].

Material	T_{melt} °C	A [MPa]	B [MPa]	C	n	M
Al 6061-t6	582	293.4	121.26	0.002	0.23	1.34

Table. 1: JOHNSON-COOK MATERIALS PROPERTIES [7]

About mesh type according to Abaqus documentation numerical complications that results in numerical problems due to meshing in models can limit the ability to obtain proper analysis results at a reasonable calculation time. Therefore new techniques are needed to optimize meshing and obtain good solutions on the other hand controlling the time of the analysis, as in many non-linear Analysis the material undergoes severe deformation, these deformations may take a lot of time to be simulated of even it may prevent the simulation from running causing the simulation to terminate.

Lagrange is this type of meshing the mesh is restricted to the material, and move with the motion of the material. With this method it is easy to track surfaces and to apply boundary condition problem [8].

Also there is Eularian, in contrast with Lagrangian analysis, in Eulerian analysis nodes are not fixed with the material however fixed with space, and material flows through mesh elements that do not deform. Eulerian elements may not always be full of material. The Eulerian material boundary must, therefore, be computed during each time increment and generally does not correspond to an element boundary. The Eulerian mesh is typically a simple rectangular grid of elements constructed to extend well beyond the Eulerian material boundaries, giving the material space in which to move and deform. If any Eulerian material moves outside the Eulerian mesh, it is not tracked by the simulation. Eulerian analyses are effective for applications involving extreme deformation, even including fluid flow [8].

Now to the type used which is the adaptive meshing technique in Abaqus combines the features of pure Lagrangian analysis and pure Eulerian analysis. This type of adaptive meshing is often referred to as Arbitrary Lagrangian-Eulerian (ALE) analysis. ALE adaptive meshing is a tool that makes it possible to maintain a high-quality mesh throughout an analysis, even when large deformation or loss of material occurs, by allowing the mesh to move independently of the material, it differs from pure Eulerian

analysis that the domain must always be filled with material [9].

Mass scaling is used in Abaqus-Explicit for better computational efficiency in dynamic analyses that contain a few very small elements that control the stable time increment. Mass scaling facto used $=10^6$ it was verified by checking its effect in increasing the kinetic energy [10].

The two plates are treated as single plate as it will not differ with the simulation if they are modeled as 2 pieces so it is modeled as a solid deformable 3D body. The length of the plate is *100 mm*, width *60 mm*, and was extruded to thickness of *1.35 mm*. Structured mesh used, element library used is Explicit, family of the elements is Coupled temperature-Displacement that has a temperature degree of freedom in addition to displacement degree of freedom, reduced integration is used, also enhanced hourglass is used to simulate severe distortion that occurs. Elements used: C3D8RT: An 8-node thermally coupled brick, trilinear displacement and temperature, reduced integration and hourglass control [11]. 19800 elements were used with 1 mm. spacing between elements.

Tool is modeled as an analytically rigid part for simplicity during this simulation to avoid node to node contact problems. Tool dimensions are as shown in the Fig. 2. Tool tilt of 1^o, penetration speed for the 1st step of *0.1 mm/sec*, tool rotational speed of *400 rpm*. For the feed step material was allowed to move with speed of *1.5 mm/sec*. Heat convection was defined for the with coefficient of *10* $W/m^2 K$ for all surfaces facing the air and of $1000W/m^2 K$ for the bottom surface to compensate the heat lost to the back plate by conduction.

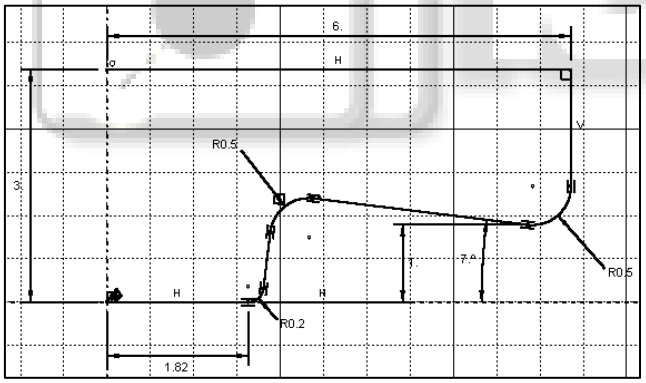

Fig. 2: Tool geometry

Surface to surface contact is applied tangential property plenty contact frictional formulation assigned, friction coefficient of *0.3* is used, a Shear stress limit = *207 MPa*.

III. EXPERIMENTAL PROCEEDURES

Same tool geometry used in the Simulation model and a plate with the same geometry. Experiment done with the following procedures; the surface for the 2 plates is cleaned with ethanol to ensure the removal of any impurities. The plate is put on the machine shown in, Pushed by 2 pressure pads. A tilt angle of *1°* is used for the tool and the machine is adjusted to work during the drilling step with *400 rpm* and downward velocity of *0.1mm/sec* and plunge depth of *0.15 mm*, dwelling for 2 seconds at *400 rpm*. Then feed at speed of *1.5 mm/sec* while tool is rotating at *400 rpm* thermal images was taken. The setting of the thermal camera measurements are shown in Fig. 3.

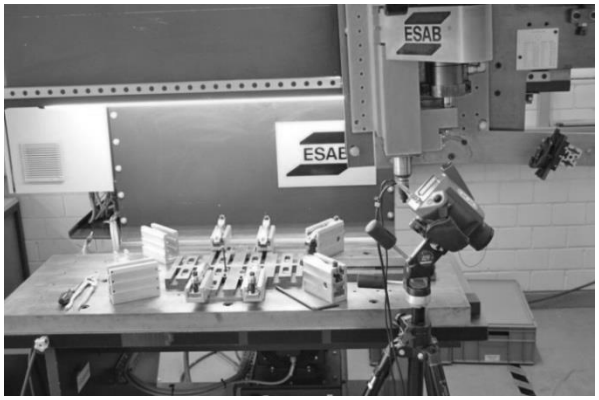

Fig. 3. Layout setting for thermal camera measurements

IV. RESULTS AND DISCUTION

A. *After Penetration Step*

Simulation ran on a 2.6 GHz computer processor, a simulation time is about 29 hours. Temperature ranges after the penetration step were simulated and the peak temperature reached was about 340 °C. A comparison is made with the distribution obtained from the experiments as shown in Fig. 4.

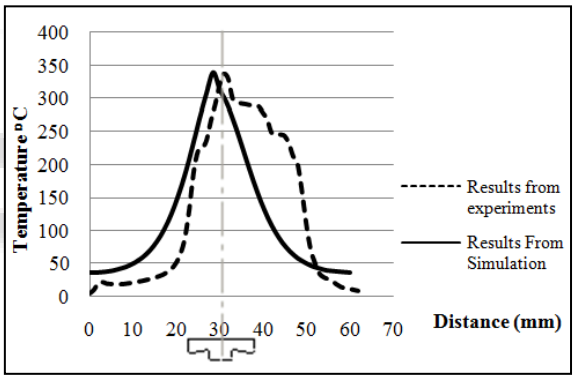

Fig. 4: Comparison between simulation and experiments after drilling

B. *After Dwelling Step*

Temperature ranges after the dwelling step were also simulated using the same simulation program and the peak temperature reached was about *270 °C*. A comparison is made with the distribution obtained from the experiments as shown in Fig. 5.

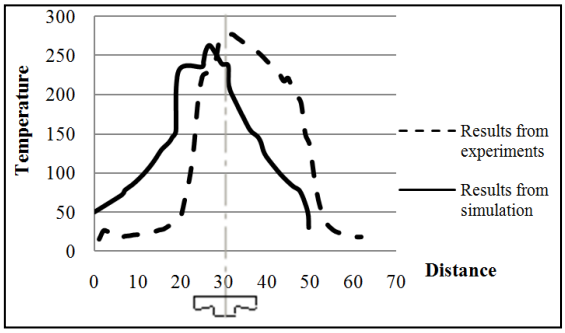

Fig. 5: Comparison between simulation and experiments after dwelling

Looking at the previous temperature distributions it is clear that the simulation of the temperature distribution quite match the temperature measurements obtained with the thermal camera. The highest temperature reached during and after the penetration step is slightly higher than the peak temperature reached right after the dwelling step. This is due to the high frictional forces imposed on the tool during the first penetration step compared to the dwelling step.

C. *During Feed Step*

Temperature ranges during the feed step is simulated using Abaqus-Explicit as shown in Fig. 6. Peak temperature reached was *450°C* during the feed step just ahead of FSW tool. The model was thermally successful and realistic, however the hole initiated was observed to be wider than the tool and a gap started to propagate behind the tool. This can be avoided by using a smaller mesh size, and further adjustment must be done with the mesh control to facilitate the numerical solution, in order to enhance the shape of the deformation and ensure that the gap behind the tool is completely filled.

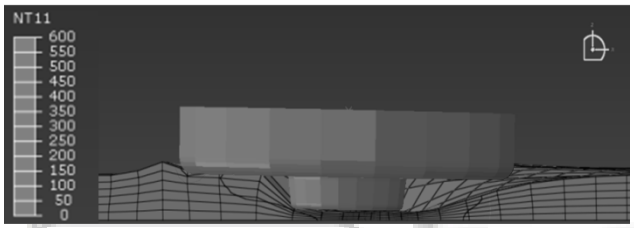

Fig. 6: Temperature Scale simulation during feed step

V. SUMMARY AND CONCLUSION

Our focus on this paper was to simulate the thermal and mechanical behavior of the FSW tool during a complete friction welding process. The results of the thermal simulation have shown realistic performance. First the maximum temperature obtained was about *450°C* which is below the melting temperature of aluminium. This means that the metal is plastically deformed rather than melted around the FSW tool. *95%* of temperature distribution obtained from the simulation around the tool was coinciding and matching to that obtained from experimental work. In the simulation of deformation in the "penetration" and "dwelling" model, the material nearly filled the gap around the tool, which means that there was a positive contact between the tool and the work piece throughout the simulation. In the "feed step" model the deformation was unrealistic and has experienced a propagation of a big gap behind the tool. It is therefore envisaged that reducing the size of the mesh and further adjusting the mesh control would result in a realistic numerical solution.

ACKNOWLEDGEMENT

The authors would like to thank the German University in Cairo for the full financial support of this project. Special thanks to Dipl.-Ing. Max Hossfeld and Dr.-Ing. Michael Seidenfuss for their guidance and supervision during out this research project at IMWF Stuttgart.

REFERENCES

[1] In The Procedure Handbook of Arc Welding, Cleveland, 1994.
[2] Kinji Higashi, "About Friction Stir Welding," 2009. [Online]. http://www.m-osaka.com/fsw/en/fsw/fsw.html.
[3] H.Shmidt and J.Hattel, "A local model for the thermomechanical conditions in friction stir welding," Process Modelling Group, Department of Manufacturing Engineering and Management,, Denmark, 2005.
[4] Abaqus Documentation, "Section 6.5.4 Fully coupled thermal-stress analysis," in Abaqus 6.11 Documentation, Simula, 2011.
[5] Abaqus Documentation, "6.3.3 Explicit dynamic analysis," in Abaqus Documentation, Simula, 2011.
[6] Y. Chao and X. Qi, "Thermal and Thermo-Mechanical Modeling of Friction Stir Welding of Aluminum Alloy 6061-T6," Journal of Materials Processing & Manufacturing Science, 1998.
[7] Leonard E.Schwer, "Aluminium plate perforation: a comparitive case study using lagrange with erosion , multimaterial ale, and smooth particle hydrodynamic," california, USA, 2009.
[8] ABAQUS documentation, "Section 14.1.1 Eulerian analysi," in Abaqus Documentation, Simula, 2011.
[9] ABQUS documentation, "Section 12.2.1 ALE adaptive meshing," in ABAQUS documentation, Simula, 2011.
[10] ABAQUS documentation, "section 11.6.1 Mass scaling," in ABAQUS documentation, 2011.
[11] ABAQUS, "27.1.4 Three-dimensional solid element library," in ABAQUS DOCUMENTATION, USA, 2011.

